Acta Mech 228, 1343–1361 (2017)
DOI 10.1007/s00707-016-1777-0

ORIGINAL PAPER

X. Chen · S. A. Meguid

Nonlinear vibration analysis of a microbeam subject to electrostatic force

Received: 17 August 2016 / Revised: 1 November 2016 / Published online: 15 December 2016

Abstract In this paper, the nonlinear vibration behavior of an electrically actuated microbeam is investigated at various levels of direct current (DC) and alternating current (AC) voltages. The governing equations are developed using Euler–Bernoulli beam theory and used to derive the frequency response of the beam. The mid-plane stretching is accounted for using von Kármán nonlinear strain, and the effects of fringing field, damping, residual axial force, and boundary conditions are also included in the model formulations. The governing equations are solved using the method of multiple scales. The results of our work reveal that the applied DC and AC voltages determine the characteristic feature of the frequency response of the microbeam. A design chart in terms of the dimensionless DC voltage and AC voltage amplitude is developed to show the domains of different characteristic frequency responses. Our results also reveal the significant effect of mid-plane stretching, damping, residual axial force, and boundary conditions on the frequency response of the microbeam. Moreover, our results further identify the effect of mid-plane stretching, damping, and residual axial force on the critical DC voltages separating the hardening and softening frequency response regions in the newly developed design chart of the micro-resonator.

1 Introduction

Micro/nano-electro-mechanical systems (MEMS/NEMS) have drawn considerable attention from the research community due to their unique advantages of small size, high precision, and low power consumption. One benchmark of MEMS/NEMS are the micro/nanobeam systems driven by electrostatic force. Various applications have been found in these systems such as switches and nonvolatile memories [1–6]. The micro/nanobeams can also be driven to vibration by an alternating current (AC) voltage. The obtained micro/nano-resonators are potential ultra-sensitive mass sensors, temperature sensors, transmitters and receivers [7–16].

The effects of the applied AC and direct current (DC) voltages on the resonance frequency of micro/nano-resonators have been largely studied in the literature. Tilmans and Legtenberg [17] derived an analytical relation between the resonance frequency and the amplitude of AC voltage, and a qualitative prediction was given. Kuang and Chen [18] developed a dynamic model for shaped microbeams with mid-plane stretching, residual axial force and fringing field effect considered. The dependence of resonance frequency on the DC voltage derived from their model agreed well with the experiments of Tilmans and Legtenberg [17]. By theoretical investigations, Jonsson et al. [19] also found that the resonance frequency of a three-terminal nano-relay can be tuned by the biased DC voltage. In the dynamic model of Jia et al. [20], Casimir force, residual axial force,

X. Chen · S. A. Meguid (✉)
Mechanics and Aerospace Design Laboratory, Department of Mechanical and Industrial Engineering, University of Toronto, 5 King's College Road, Toronto, ON M5S 3G8, Canada
E-mail: meguid@mie.utoronto.ca
Tel.: +1 416 978 5741
Fax: +1 416 978 7753

mid-plane stretching, and fringing field effect were taken into account. The resonance frequencies at different levels of AC voltage amplitude were derived and quantitatively agreed with the experiments of Tilmans and Legtenberg [17].

Experiments on the vibration behavior of micro/nano-resonators have also been reported in the literature, and frequency response curves of linear, hardening, and softening characteristics have all been observed [17,21–28]. The nonlinearity in the vibration behavior of the micro/nano-resonator is mainly due to: (i) the electrostatic and intermolecular forces which are nonlinear functions of beam deflection, and (ii) the geometrical nonlinearity from mid-plane stretching. The former one has a softening effect on the micro/nanobeam, while the latter one has a hardening effect [20]. In the remainder of this paper, the frequency response associated with the hardening effect on the micro/nanobeam will be named "hardening frequency response," while that associated with the softening effect will be termed "softening frequency response."

Theoretical studies on the vibration behavior of micro/nano-resonators can also be found in the literature. With the hardening effect considered, Gui et al. [29] proposed a criterion on AC and DC voltages for the linear vibration of a clamped–clamped microbeam. Based on the dynamic model, Rhoads et al. [30] revealed that the nonlinear frequency response of a microbeam subjected to a symmetric electrostatic actuation depends on AC and DC voltages. Kacem et al. [31] developed a quasi-analytical model for the nonlinear vibration of a clamped–clamped microbeam and found hardening frequency response in the simulated cases. The vibration behavior of a micro-cantilever near the half natural frequency has been studied in [32–34]. The dynamic pull-in has been found, and the effects of damping, fringing field and AC voltage amplitude on the frequency response have also been studied. Ouakad et al. [35] simulated the dynamic behavior of an initially curved microbeam and found softening frequency response at the studied levels of AC and DC voltages. Kim et al. [36] developed a dynamic model for a nano-cantilever with a tip mass at the free end and studied the effect of the inertial nonlinearity of the tip mass on the frequency response. Ruzziconi et al. [28] considered the imperfect beam shape (e.g., curled-up profile) in their dynamic model and predicted a softening frequency response when increasing the AC voltage amplitude at a fixed level of DC voltage.

A careful literature review indicates that most studies are conducted at a certain level of AC and DC voltages, and one characteristic feature (i.e., linear, hardening or softening) of the vibration behavior of the micro/nano-resonator is observed. Studies concerned with characterizing the vibration behavior of a general micro/nano-resonator at various levels of AC and DC voltages are seldom reported. Moreover, studies on determining the parameters which govern the vibration characteristics are also limited.

In this paper, we extend the earlier work to study the vibration behavior of a general micro-resonator at various levels of AC and DC voltages. A design chart in terms of dimensionless AC and DC voltages is developed to show the regions of linear, hardening, and softening frequency responses. The effects of the governing parameters on the frequency response and the design chart of the micro-resonator are further investigated. The studied governing parameters include: mid-plane stretching, fringing field effect, damping effect, residual axial force, and boundary conditions.

2 Model formulation

2.1 Governing equation

A rectangular microbeam of length L, width b, and thickness h is actuated by a distributed electrostatic force, as depicted in Fig. 1. Applying the Euler–Bernoulli beam theory for a thin beam ($h << L$) and further using

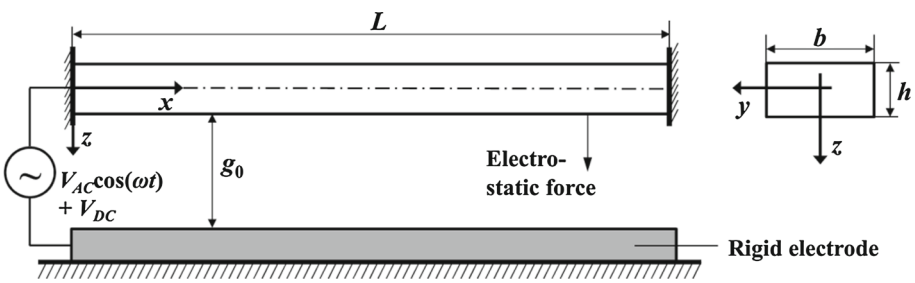

Fig. 1 Microbeam actuated by a distributed electrostatic force along z-coordinate

the von Kármán nonlinear strain to take into account the mid-plane stretching, we calculate the nonzero strain component as [37]:

$$\varepsilon_{xx} = \frac{\partial u(x,t)}{\partial x} - z\frac{\partial^2 w(x,t)}{\partial x^2} + \frac{1}{2}\left(\frac{\partial w(x,t)}{\partial x}\right)^2 \tag{1}$$

where t is time, u and w are respectively the axial (along x-coordinate) and transverse (along z) displacements of a point on the mid-plane of the beam. The variation δU_{elas} of the elastic strain energy is derived from Eq. (1) as:

$$\begin{aligned}\delta U_{\text{elas}} &= \int_0^L \int_S (\sigma_{xx}\delta\varepsilon_{xx})\mathrm{d}s\mathrm{d}x \\ &= -\int_0^L \frac{\partial N(x,t)}{\partial x}\delta u\mathrm{d}x - \int_0^L \left(\frac{\partial^2 M(x,t)}{\partial x^2} + \frac{\partial}{\partial x}\left(N(x,t)\frac{\partial w}{\partial x}\right)\right)\delta w\mathrm{d}x \\ &\quad + N(x,t)\delta u|_{x=0}^{L} + \left(\frac{\partial M(x,t)}{\partial x} + N(x,t)\frac{\partial w}{\partial x}\right)\delta w\Big|_{x=0}^{L} - M(x,t)\frac{\partial \delta w}{\partial x}\Big|_{x=0}^{L}\end{aligned} \tag{2}$$

where $\int_S \mathrm{d}s$ is the integral over the cross section, i.e., $y-z$ plane in Fig. 1; the axial force N and the bending moment M are given below:

$$N = \int_S \sigma_{xx}\mathrm{d}s, \tag{3.1}$$

$$M = \int_S z\sigma_{xx}\mathrm{d}s. \tag{3.2}$$

For a thin beam, the axial displacement u and the beam curvature $\frac{\partial^2 w}{\partial x^2}$ are negligible with respect to the transverse displacement w. Therefore, we calculate the variation δE_{k} of the kinetic energy as:

$$\delta E_{\text{k}} = \int_0^L \rho S\left(\frac{\partial w}{\partial t}\frac{\partial \delta w}{\partial t}\right)\mathrm{d}x \tag{4}$$

where ρ is the mass density and $S(=bh)$ is the cross-sectional area. The variation δW_{ext} of the work done by the external forces is expressed as:

$$\delta W_{\text{ext}} = \int_0^L (f_{\text{damp}} + f_{\text{elec}})\delta w\mathrm{d}x \tag{5}$$

where the viscous damping force f_{damp} can be estimated as:

$$f_{\text{damp}} = -c_{\text{d}}\frac{\partial w}{\partial t} \tag{6}$$

with c_{d} being the damping coefficient per unit length, and the electrostatic force f_{elec} with fringing field considered by Palmer's formula [38] is calculated as [32,39]:

$$f_{\text{elec}} = \frac{1}{2}\frac{\varepsilon_0 b\,(V_{\text{DC}} + V_{\text{AC}}\cos(\omega t))^2}{(g_0 - w)^2}\left(1 + 0.65\frac{g_0 - w}{b}\right) \tag{7}$$

with ε_0 being the vacuum permittivity ($=8.8542\times 10^{-12}\,\text{F}\,\text{m}^{-1}$), g_0 being the initial gap between the beam and the rigid electrode, as depicted in Fig. 1, V_{DC} being the applied DC voltage, and V_{AC} being the amplitude of the applied AC voltage with the angular velocity, ω. By introducing Eqs. (2), (4), and (5) into the following Hamilton's principle:

$$\int_0^{t_1} (\delta E_{\text{k}} + \delta W_{\text{ext}} - \delta U_{\text{elas}})\,\mathrm{d}t = 0 \tag{8}$$

and further integrating the result by parts with respect to t and x, we have:

$$\int_0^{t_1}\int_0^{L}\frac{\partial N}{\partial x}\delta u\mathrm{d}x\mathrm{d}t+\int_0^{t_1}\int_0^{L}\left(\frac{\partial^2 M}{\partial x^2}+\frac{\partial}{\partial x}\left(N\frac{\partial w}{\partial x}\right)+f_{\mathrm{damp}}+f_{\mathrm{elec}}-\rho S\frac{\partial^2 w}{\partial t^2}\right)\delta w\mathrm{d}x\mathrm{d}t$$
$$+\int_0^{t_1}\left(-N\delta u-\left(\frac{\partial M}{\partial x}+N\frac{\partial w}{\partial x}\right)\delta w+M\frac{\partial\delta w}{\partial x}\right)_{x=0}^{L}\mathrm{d}t+\int_0^{L}\left(\rho S\frac{\partial w}{\partial t}\delta w\right)_{t=0}^{t_1}\mathrm{d}x=0. \tag{9}$$

The following governing equations can be obtained from Eq. (9):

$$\delta u\colon \frac{\partial N}{\partial x}=0, \tag{10.1}$$
$$\delta w\colon \frac{\partial^2 M}{\partial x^2}+\frac{\partial}{\partial x}\left(N\frac{\partial w}{\partial x}\right)+f_{\mathrm{damp}}+f_{\mathrm{elec}}-\rho S\frac{\partial^2 w}{\partial t^2}=0. \tag{10.2}$$

Suppose that the beam material is elastically isotropic with Young's modulus E and Poisson's ratio ν. Then the 1D constitutive relation becomes:

$$\sigma_{xx}=E^*\varepsilon_{xx} \tag{11}$$

where the effective Young's modulus E^* is $\frac{E}{1-\nu^2}$ for a wide beam ($b>5h$) considered here. With Eqs. (1) and (11), Eq. (3) can be rewritten as:

$$N=E^*S\left(\frac{\partial u}{\partial x}+\frac{1}{2}\left(\frac{\partial w}{\partial x}\right)^2\right), \tag{12.1}$$
$$M=-E^*I\frac{\partial^2 w}{\partial x^2}. \tag{12.2}$$

Equation (10.1) shows that N is constant along the x-coordinate. By estimating N as the average value of Eq. (12.1), considering the boundary conditions of clamped–clamped beam, i.e., $u(0)=u(L)=0$, and further including a residual axial force P from fabrication or temperature variation, we obtain:

$$N=\frac{E^*S}{2L}\left(\int_0^{L}\left(\frac{\partial w}{\partial x}\right)^2\mathrm{d}x\right)+P. \tag{13}$$

With Eqs. (6), (7), (10.1), (12.2) and (13), Eq. (10.2) can be rewritten as:

$$\rho S\frac{\partial^2 w}{\partial t^2}+c_{\mathrm{d}}\frac{\partial w}{\partial t}+E^*I\frac{\partial^4 w}{\partial x^4}-\left(P+\frac{E^*S}{2L}\left(\int_0^{L}\left(\frac{\partial w}{\partial x}\right)^2\mathrm{d}x\right)\right)\frac{\partial^2 w}{\partial x^2},$$
$$=\frac{1}{2}\frac{\varepsilon_0 b\left(V_{\mathrm{DC}}+V_{\mathrm{AC}}\cos(\omega t)\right)^2}{(g_0-w)^2}\left(1+0.65\frac{g_0-w}{b}\right). \tag{14}$$

Introducing the dimensionless quantities in Table 1, we obtain the following dimensionless governing equation from Eq. (14):

$$\frac{\partial^2\overline{w}}{\partial\overline{t}^2}+\overline{c_{\mathrm{d}}}\frac{\partial\overline{w}}{\partial\overline{t}}+\frac{\partial^4\overline{w}}{\partial\overline{x}^4}-\overline{P}\frac{\partial^2\overline{w}}{\partial\overline{x}^2}-\alpha\left(\int_0^{1}\left(\frac{\partial\overline{w}}{\partial\overline{x}}\right)^2\mathrm{d}\overline{x}\right)\frac{\partial^2\overline{w}}{\partial\overline{x}^2}$$
$$=\left(\overline{V_{\mathrm{DC}}}+\overline{V_{\mathrm{AC}}}\cos(\overline{\omega}\overline{t})\right)^2\left(\frac{1}{(1-\overline{w})^2}+\frac{\beta}{(1-\overline{w})}\right). \tag{15}$$

The dimensionless boundary conditions of clamped–clamped beam are:

$$\delta\overline{w}:\overline{w}(0,\overline{t})=0,\quad \overline{w}(1,\overline{t})=0, \tag{16.1}$$
$$\frac{\partial\delta\overline{w}}{\partial\overline{x}}:\frac{\partial\overline{w}}{\partial\overline{x}}(0,\overline{t})=0,\quad \frac{\partial\overline{w}}{\partial\overline{x}}(1,\overline{t})=0. \tag{16.2}$$

Table 1 Dimensionless quantities

Quantity	Expression	Meaning
$\overline{c_\mathrm{d}}$	$c_\mathrm{d}L^2/\sqrt{E^*I\rho S}$	Dimensionless damping coefficient
$\overline{P}$	$PL^2/(E^*I)$	Dimensionless residual axial force
$\bar{t}$	$t/\sqrt{\rho SL^4/(E^*I)}$	Dimensionless time
$\overline{V_\mathrm{AC}}$	$V_\mathrm{AC}/\sqrt{E^*h^3g_0^3/(6\varepsilon_0L^4)}$	Dimensionless AC voltage amplitude
$\overline{V_\mathrm{DC}}$	$V_\mathrm{DC}/\sqrt{E^*h^3g_0^3/(6\varepsilon_0L^4)}$	Dimensionless DC voltage
$\overline{w}$	w/g_0	Dimensionless deflection
$\overline{x}$	x/L	Normalized coordinate
α	$6\,(g_0/h)^2$	Stretching parameter
β	$0.65\,(g_0/b)$	Fringing field parameter
$\overline{\omega}$	$\omega/\sqrt{E^*I/(\rho SL^4)}$	Dimensionless angular frequency

2.2 Analytical model of frequency response

The micro-resonator is usually actuated by low V_DC and V_AC to vibrate at small amplitude with weak damping effect. In this case, the method of multiple scales can be adopted [32,35]. Considering small amplitude, weak damping, and nonlinear effects, we expand the electrostatic force around $\overline{w}=0$ in Eq. (15) and set the electrostatic force, damping and mid-plane stretching terms [2nd and 5th on the left-hand-side of Eq. (15)] to a slow scale by multiplying them by a small bookkeeping parameter ξ:

$$\frac{\partial^2\overline{w}}{\partial\bar{t}^2}+\xi\overline{c_\mathrm{d}}\frac{\partial\overline{w}}{\partial\bar{t}}+\frac{\partial^4\overline{w}}{\partial\overline{x}^4}-\overline{P}\frac{\partial^2\overline{w}}{\partial\overline{x}^2}-\xi\alpha\left(\int_0^1\left(\frac{\partial\overline{w}}{\partial\overline{x}}\right)^2\mathrm{d}\overline{x}\right)\frac{\partial^2\overline{w}}{\partial\overline{x}^2}$$
$$=\xi\left(\overline{V_\mathrm{DC}}+\overline{V_\mathrm{AC}}\cos(\overline{\omega}\bar{t})\right)^2\left(1+\beta+(2+\beta)\,\overline{w}+(3+\beta)\,\overline{w}^2+(4+\beta)\,\overline{w}^3\right). \tag{17}$$

By introducing into Eqs. (16) and (17) the following first-order expansion of $\overline{w}$:

$$\overline{w}=\overline{w}_0(\overline{x},T_0,T_1)+\xi\overline{w}_1(\overline{x},T_0,T_1) \tag{18}$$

with $T_0(=\bar{t})$ being a fast timescale and $T_1(=\xi\bar{t})$ being a slow timescale, and further equating the like powers of ξ, we obtain:
Order ξ^0:

$$\frac{\partial^2\overline{w}_0}{\partial T_0^2}+\frac{\partial^4\overline{w}_0}{\partial\overline{x}^4}-\overline{P}\frac{\partial^2\overline{w}_0}{\partial\overline{x}^2}=0, \tag{19.1}$$

$$\overline{w}_0(0,T_0,T_1)=0,\ \overline{w}_0(1,T_0,T_1)=0,\ \frac{\partial\overline{w}_0}{\partial\overline{x}}(0,T_0,T_1)=0,\ \frac{\partial\overline{w}_0}{\partial\overline{x}}(1,T_0,T_1)=0; \tag{19.2}$$

Order ξ^1:

$$\frac{\partial^2\overline{w}_1}{\partial T_0^2}+\frac{\partial^4\overline{w}_1}{\partial\overline{x}^4}-\overline{P}\frac{\partial^2\overline{w}_1}{\partial\overline{x}^2}=-2\frac{\partial^2\overline{w}_0}{\partial T_0\partial T_1}-\overline{c_\mathrm{d}}\frac{\partial\overline{w}_0}{\partial T_0}+\alpha\left(\int_0^1\left(\frac{\partial\overline{w}_0}{\partial\overline{x}}\right)^2\mathrm{d}\overline{x}\right)\frac{\partial^2\overline{w}_0}{\partial\overline{x}^2}$$
$$+\left(\overline{V_\mathrm{DC}}+\overline{V_\mathrm{AC}}\cos(\overline{\omega}T_0)\right)^2\left(1+\beta+(2+\beta)\,\overline{w}_0+(3+\beta)\,\overline{w}_0^2+(4+\beta)\,\overline{w}_0^3\right), \tag{20.1}$$

$$\overline{w}_1(0,T_0,T_1)=0,\ \overline{w}_1(1,T_0,T_1)=0,\ \frac{\partial\overline{w}_1}{\partial\overline{x}}(0,T_0,T_1)=0,\ \frac{\partial\overline{w}_1}{\partial\overline{x}}(1,T_0,T_1)=0. \tag{20.2}$$

The solution to Eq. (19) is supposed to be:

$$\overline{w}_0=\phi_j(\overline{x})\left(A(T_1)\mathrm{e}^{i\omega_jT_0}+A^*(T_1)\mathrm{e}^{-i\omega_jT_0}\right) \tag{21}$$

with A being a coefficient depending on the slow timescale T_1 and A^* being its complex conjugate; $\phi_j\,(j=1,2,\ldots,n)$ being the jth linear undamped vibration mode of the clamped–clamped beam:

$$\phi_j(\overline{x})=C_j\left(\cos h(\lambda_j\overline{x})-\cos(\lambda_j\overline{x})-\frac{\sin h(\lambda_j)+\sin(\lambda_j)}{\cos h(\lambda_j)-\cos(\lambda_j)}\left(\sin h(\lambda_j\overline{x})-\sin(\lambda_j\overline{x})\right)\right). \tag{22}$$

In Eq. (22), C_j is a constant satisfying $\max_{\overline{x}\in[0,1]}\left|\phi_j(\overline{x})\right| = 1$, and λ_j is a frequency parameter satisfying $\cos h(\lambda_j)\cos(\lambda_j) = 1$. λ_j is related to the resonance angular frequency ω_j at the residual axial force $\overline{P}$ by:

$$\omega_j = \sqrt{\lambda_j^4 - \overline{P}s_{jj}/m_{jj}} \tag{23}$$

where $m_{jj} = \int_0^1 \phi_j^2 \mathrm{d}\overline{x}$, $s_{jj} = \int_0^1 \phi_j\phi_j{}''\mathrm{d}\overline{x}$, and a superimposed apostrophe denotes a derivative with respect to the normalized coordinate $\overline{x}$. The micro-resonator usually works near the primary resonance regime, so the first vibration mode is considered here, i.e., $j = 1$ in Eqs. (21)–(23). To indicate the nearness of the applied frequency $\overline{\omega}$ to the primary resonance frequency ω_1, a detuning parameter δ is introduced:

$$\overline{\omega} = \omega_1 + \xi\delta. \tag{24}$$

The square of the applied voltages can be expressed as:

$$\left(\overline{V_{\mathrm{DC}}} + \overline{V_{\mathrm{AC}}}\cos(\overline{\omega}T_0)\right)^2 = \overline{V_{\mathrm{DC}}}^2 + \frac{1}{2}\overline{V_{\mathrm{AC}}}^2 + 2\overline{V_{\mathrm{DC}}V_{\mathrm{AC}}}\cos(\overline{\omega}T_0) + \frac{1}{2}\overline{V_{\mathrm{AC}}}^2\cos(2\overline{\omega}T_0). \tag{25}$$

Equation (25) shows that the microbeam can vibrate at the frequency of $\overline{\omega}$ or $2\overline{\omega}$, depending on the levels of $\overline{V_{\mathrm{DC}}}$ and $\overline{V_{\mathrm{AC}}}$. In this study, we only consider the most common case where $\overline{V_{\mathrm{DC}}} > \overline{V_{\mathrm{AC}}}$ and the microbeam vibrates at $\overline{\omega}$. Then by neglecting $\overline{V_{\mathrm{AC}}}^2$ in Eq. (25) and introducing Eq. (24), we have:

$$\left(\overline{V_{\mathrm{DC}}} + \overline{V_{\mathrm{AC}}}\cos(\overline{\omega}T_0)\right)^2 \approx \overline{V_{\mathrm{DC}}}^2 + \overline{V_{\mathrm{DC}}V_{\mathrm{AC}}}\left(\mathrm{e}^{i(\omega_1 T_0 + T_1\delta)} + \mathrm{e}^{-i(\omega_1 T_0 + T_1\delta)}\right). \tag{26}$$

With Eqs. (21) and (26), Eq. (20.1) can be rewritten as:

$$\begin{aligned}\frac{\partial^2\overline{w}_1}{\partial T_0^2} + \frac{\partial^4\overline{w}_1}{\partial\overline{x}^4} - \overline{P}\frac{\partial^2\overline{w}_1}{\partial\overline{x}^2} = c_0 + \left(c_1\mathrm{e}^{i\omega_1 T_0} + c_1^*\mathrm{e}^{-i\omega_1 T_0}\right) + \left(c_2\mathrm{e}^{i(2\omega_1 T_0)} + c_2^*\mathrm{e}^{-i(2\omega_1 T_0)}\right)\\ + \left(c_3\mathrm{e}^{i(3\omega_1 T_0)} + c_3^*\mathrm{e}^{-i(3\omega_1 T_0)}\right) + \left(c_4\mathrm{e}^{i(4\omega_1 T_0)} + c_4^*\mathrm{e}^{-i(4\omega_1 T_0)}\right).\end{aligned} \tag{27}$$

c_0–c_4 are coefficients and c_1^*–c_4^* are the complex conjugates of c_1–c_4. c_1 is calculated as:

$$\begin{aligned}c_1 = &-2i\omega_1\phi_1\frac{\mathrm{d}A}{\mathrm{d}T_1} - i\overline{c_{\mathrm{d}}}\omega_1\phi_1 A + 3\alpha\phi_1{}''\left(\int_0^1 (\phi_1{}')^2\,\mathrm{d}\overline{x}\right)A^2A^* + (2+\beta)\,\overline{V_{\mathrm{DC}}}^2\phi_1 A\\ &+ 3\,(4+\beta)\,\overline{V_{\mathrm{DC}}}^2\phi_1^3A^2A^* + (1+\beta)\,\overline{V_{\mathrm{DC}}V_{\mathrm{AC}}}\mathrm{e}^{iT_1\delta} + 2\,(3+\beta)\,\overline{V_{\mathrm{DC}}V_{\mathrm{AC}}}\phi_1^2AA^*\mathrm{e}^{iT_1\delta}\\ &+ (3+\beta)\,\overline{V_{\mathrm{DC}}V_{\mathrm{AC}}}\phi_1^2A^2\mathrm{e}^{-iT_1\delta}.\end{aligned} \tag{28}$$

To satisfy the solvability condition where the right-hand-side of Eq. (27) must be orthogonal to any solution of Eq. (19) [32], we derive:

$$c_1\phi_1 = 0. \tag{29}$$

By introducing Eq. (28) into Eq. (29) and integrating the result from $\overline{x} = 0$ to 1, we have:

$$\begin{aligned}&-2i\omega_1 m_2\frac{\mathrm{d}A}{\mathrm{d}T_1} - i\overline{c_{\mathrm{d}}}\omega_1 m_2 A + 3\alpha s_1A^2A^* + (2+\beta)\,\overline{V_{\mathrm{DC}}}^2 m_2A + 3\,(4+\beta)\,\overline{V_{\mathrm{DC}}}^2 m_4A^2A^*\\ &+ (1+\beta)\,\overline{V_{\mathrm{DC}}V_{\mathrm{AC}}}m_1\mathrm{e}^{iT_1\delta} + 2\,(3+\beta)\,\overline{V_{\mathrm{DC}}V_{\mathrm{AC}}}m_3AA^*\mathrm{e}^{iT_1\delta} + (3+\beta)\,\overline{V_{\mathrm{DC}}V_{\mathrm{AC}}}m_3A^2\mathrm{e}^{-iT_1\delta} = 0\end{aligned} \tag{30}$$

with the parameters being:

$$\begin{aligned}&m_1 = \int_0^1\phi_1\mathrm{d}\overline{x},\ m_2 = \int_0^1\phi_1^2\mathrm{d}\overline{x},\ m_3 = \int_0^1\phi_1^3\mathrm{d}\overline{x},\ m_4 = \int_0^1\phi_1^4\mathrm{d}\overline{x},\\ &s_1 = \left(\int_0^1(\phi_1{}')^2\,\mathrm{d}\overline{x}\right)\left(\int_0^1\phi_1\phi_1{}''\mathrm{d}\overline{x}\right).\end{aligned} \tag{31}$$

Introducing into Eq. (30) the following polar form of $A(T_1)$:

$$A(T_1) = \frac{1}{2}a(T_1)\mathrm{e}^{i\theta(T_1)} \tag{32}$$

with a being the vibration amplitude, separating the real and imaginary parts, and further introducing the phase lag $\gamma = T_1\delta - \theta$, we obtain:

$$\frac{\mathrm{d}a}{\mathrm{d}T_1} = -\frac{\overline{c_\mathrm{d}}}{2}a + \left(\frac{m_1}{m_2\omega_1}(1+\beta) + \frac{m_3}{4m_2\omega_1}(3+\beta)a^2\right)\overline{V_\mathrm{DC}V_\mathrm{AC}}\sin\gamma, \tag{33.1}$$

$$a\frac{\mathrm{d}\gamma}{\mathrm{d}T_1} = a\delta + \frac{1}{2\omega_1}(2+\beta)\,\overline{V_\mathrm{DC}}^2 a + \frac{3\alpha s_1}{8m_2\omega_1}a^3 + \frac{3m_4}{8m_2\omega_1}(4+\beta)\,\overline{V_\mathrm{DC}}^2 a^3 + \left(\frac{m_1}{m_2\omega_1}(1+\beta) + \frac{3m_3}{4m_2\omega_1}(3+\beta)a^2\right)\overline{V_\mathrm{DC}V_\mathrm{AC}}\cos\gamma. \tag{33.2}$$

For a steady response $\frac{\mathrm{d}a}{\mathrm{d}T_1} = 0$ and $\frac{\mathrm{d}\gamma}{\mathrm{d}T_1} = 0$, we can reduce Eq. (33) to:

$$\left(\frac{m_1}{m_2\omega_1}(1+\beta) + \frac{m_3}{4m_2\omega_1}(3+\beta)a^2\right)\overline{V_\mathrm{DC}V_\mathrm{AC}}\sin\gamma = \frac{\overline{c_\mathrm{d}}}{2}a, \tag{34.1}$$

$$\left(\frac{m_1}{m_2\omega_1}(1+\beta) + \frac{3m_3}{4m_2\omega_1}(3+\beta)a^2\right)\overline{V_\mathrm{DC}V_\mathrm{AC}}\cos\gamma = -a\delta - \frac{1}{2\omega_1}(2+\beta)\,\overline{V_\mathrm{DC}}^2 a - \frac{3\alpha s_1}{8m_2\omega_1}a^3 - \frac{3m_4}{8m_2\omega_1}(4+\beta)\,\overline{V_\mathrm{DC}}^2 a^3. \tag{34.2}$$

Equation (34) leads to:

$$\begin{aligned} &b_1^2b_3^2a^{10} + \left(2b_1^2b_3b_4 + 2b_1b_2b_3^2 - 9b_1^4b_6^2\right)a^8 \\ &+ \left(b_1^2b_4^2 + 4b_1b_2b_3b_4 + b_2^2b_3^2 + 9b_1^2b_5^2 - 24b_1^3b_2b_6^2\right)a^6 \\ &+ \left(2b_1b_2b_4^2 + 2b_2^2b_3b_4 + 6b_1b_2b_5^2 - 22b_1^2b_2^2b_6^2\right)a^4 \\ &+ \left(b_2^2b_4^2 + b_2^2b_5^2 - 8b_1b_2^3b_6^2\right)a^2 - b_2^4b_6^2 = 0, \end{aligned} \tag{35.1}$$

$$\gamma = \arccos\left(-\frac{\left(b_4a + b_3a^3\right)}{b_6\left(b_2 + 3b_1a^2\right)}\right) \tag{35.2}$$

with the coefficients being:

$$b_1 = \frac{m_3}{4m_2\omega_1}(3+\beta), \quad b_2 = \frac{m_1}{m_2\omega_1}(1+\beta), \quad b_3 = \frac{3\alpha s_1}{8m_2\omega_1} + \frac{3m_4}{8m_2\omega_1}(4+\beta)\,\overline{V_\mathrm{DC}}^2,$$
$$b_4 = \delta + \frac{1}{2\omega_1}(2+\beta)\,\overline{V_\mathrm{DC}}^2, \quad b_5 = \frac{\overline{c_\mathrm{d}}}{2}, \quad b_6 = \overline{V_\mathrm{DC}V_\mathrm{AC}}. \tag{36}$$

A quality factor Q is commonly used to study the damping effect. In this case, the dimensionless damping coefficient $\overline{c_\mathrm{d}}$ in Eqs. (15) and (35) can be replaced with the following relation to Q [40]:

$$\overline{c_\mathrm{d}} = \frac{\omega_1}{Q}. \tag{37}$$

Equation (35) is the analytical model for the frequency response of the microbeam. By solving Eq. (35.1) at different levels of the detuning parameter δ, we can obtain the evolution of the maximum beam deflection (normalized as the dimensionless vibration amplitude a) with the applied dimensionless angular frequency $\overline{\omega}$ (using Eq. (24) with $\xi = 1$). To analyze the stability of each point (δ_0, a_0) on the frequency response curve, the following procedures are adopted. We introduce $\delta = \delta_0$ and $a = a_0$ into Eq. (35.2) and solve the resulting equation to obtain the phase lag γ_0. Further introducing γ_0 and a_0 into the following Jacobian matrix J_a of Eq. (33):

$$J_a = \begin{bmatrix} \frac{\partial(\mathrm{d}a/\mathrm{d}T_1)}{\partial a} & \frac{\partial(\mathrm{d}a/\mathrm{d}T_1)}{\partial\gamma} \\ \frac{\partial(\mathrm{d}\gamma/\mathrm{d}T_1)}{\partial a} & \frac{\partial(\mathrm{d}\gamma/\mathrm{d}T_1)}{\partial\gamma} \end{bmatrix} = \begin{bmatrix} -b_5 + 2b_1b_6a\sin\gamma & \left(b_2 + b_1a^2\right)b_6\cos\gamma \\ 2b_3a - \left(\frac{b_2}{a^2} - 3b_1\right)b_6\cos\gamma & -\left(\frac{b_2}{a} + 3b_1a\right)b_6\sin\gamma \end{bmatrix} \tag{38}$$

will enable us to calculate the eigenvalues of J_a. If the real parts of all the eigenvalues are negative, the point (δ_0, a_0) is stable; otherwise, it is unstable.

2.3 Numerical simulation

In order to validate the steady-state frequency response obtained from the analytical model of Eq. (35.1), we solve the governing equation (15) with the boundary conditions in Eq. (16) to obtain the time evolution of the beam deflection at each frequency. The Galerkin decomposition method is used [20,28,30,35,36]:

$$\overline{w} = \sum_{j=1}^{n} q_j(\overline{t})\phi_j(\overline{x}) \tag{39}$$

where $\phi_j (j = 1, 2, \ldots, n)$ is the jth linear undamped vibration mode, which is given in Eq. (22), and q_j is the generalized coordinate. We multiply Eq. (15) by $(1 - \overline{w})^2$, introduce Eq. (39), further multiply the resulting equation by $\phi_i (i = 1, 2, \ldots, n)$, and integrate from $\overline{x} = 0$ to 1 to obtain the following n-degree-of-freedom reduced-order model:

$$\begin{aligned}
&\left(\int_0^1 \phi_i^2 \mathrm{d}\overline{x}\right)\ddot{q}_i - 2\sum_{j=1}^{n}\sum_{k=1}^{n}\left(\int_0^1 \phi_k\phi_j\phi_i \mathrm{d}\overline{x}\right) q_k\ddot{q}_j + \sum_{j=1}^{n}\sum_{k=1}^{n}\sum_{l=1}^{n}\left(\int_0^1 \phi_l\phi_k\phi_j\phi_i \mathrm{d}\overline{x}\right) q_l q_k\ddot{q}_j + \overline{c_\mathrm{d}}\left(\int_0^1 \phi_i^2 \mathrm{d}\overline{x}\right)\dot{q}_i \\
&- 2\overline{c_\mathrm{d}}\sum_{j=1}^{n}\sum_{k=1}^{n}\left(\int_0^1 \phi_k\phi_j\phi_i \mathrm{d}\overline{x}\right) q_k\dot{q}_j + \overline{c_\mathrm{d}}\sum_{j=1}^{n}\sum_{k=1}^{n}\sum_{l=1}^{n}\left(\int_0^1 \phi_l\phi_k\phi_j\phi_i \mathrm{d}\overline{x}\right) q_l q_k\dot{q}_j + \lambda_i^4\left(\int_0^1 \phi_i^2 \mathrm{d}\overline{x}\right) q_i \\
&- 2\sum_{j=1}^{n}\sum_{k=1}^{n}\left(\int_0^1 \phi_k\phi_j\phi_i \mathrm{d}\overline{x}\right)\lambda_j^4 q_k q_j + \sum_{j=1}^{n}\sum_{k=1}^{n}\sum_{l=1}^{n}\left(\int_0^1 \phi_l\phi_k\phi_j\phi_i \mathrm{d}\overline{x}\right)\lambda_j^4 q_l q_k q_j \\
&- \left(\overline{P} + \alpha\sum_{j=1}^{n}\sum_{k=1}^{n}\left(\int_0^1 \phi_k{}'\phi_j{}' \mathrm{d}\overline{x}\right) q_k q_j\right)\left(\sum_{j=1}^{n}\left(\int_0^1 \phi_j{}''\phi_i \mathrm{d}\overline{x}\right) q_j - 2\sum_{j=1}^{n}\sum_{k=1}^{n}\left(\int_0^1 \phi_k\phi_j{}''\phi_i \mathrm{d}\overline{x}\right) q_k q_j\right. \\
&\left. + \sum_{j=1}^{n}\sum_{k=1}^{n}\sum_{l=1}^{n}\left(\int_0^1 \phi_l\phi_k\phi_j{}''\phi_i \mathrm{d}\overline{x}\right) q_l q_k q_j\right) = \left(\overline{V_\mathrm{DC}} + \overline{V_\mathrm{AC}}\cos(\overline{\omega}\overline{t})\right)^2\left((1+\beta)\int_0^1 \phi_i \mathrm{d}\overline{x} - \beta\left(\int_0^1 \phi_i^2 \mathrm{d}\overline{x}\right) q_i\right) \\
&\text{for } i = 1, 2, \ldots, n
\end{aligned} \tag{40}$$

where an over dot denotes a derivative with respect to the normalized time $\overline{t}$. Using the following variables:

$$q_{i0} = q_i, \tag{41.1}$$

$$q_{i1} = \dot{q}_i \tag{41.2}$$

we have:

$$\dot{q}_{i0} = q_{i1}, \tag{42.1}$$

$$\dot{q}_{i1} = \ddot{q}_i. \tag{42.2}$$

With Eqs. (41) and (42.2), Eq. (40) can be rewritten as:

$$\begin{aligned}
&\left(\int_0^1 \phi_i^2 \mathrm{d}\overline{x}\right)\dot{q}_{i1} - 2\sum_{j=1}^{n}\sum_{k=1}^{n}\left(\int_0^1 \phi_k\phi_j\phi_i \mathrm{d}\overline{x}\right) q_{k0}\dot{q}_{j1} + \sum_{j=1}^{n}\sum_{k=1}^{n}\sum_{l=1}^{n}\left(\int_0^1 \phi_l\phi_k\phi_j\phi_i \mathrm{d}\overline{x}\right) q_{l0}q_{k0}\dot{q}_{j1} + \overline{c_\mathrm{d}}\left(\int_0^1 \phi_i^2 \mathrm{d}\overline{x}\right) q_{i1} \\
&- 2\overline{c_\mathrm{d}}\sum_{j=1}^{n}\sum_{k=1}^{n}\left(\int_0^1 \phi_k\phi_j\phi_i \mathrm{d}\overline{x}\right) q_{k0}q_{j1} + \overline{c_\mathrm{d}}\sum_{j=1}^{n}\sum_{k=1}^{n}\sum_{l=1}^{n}\left(\int_0^1 \phi_l\phi_k\phi_j\phi_i \mathrm{d}\overline{x}\right) q_{l0}q_{k0}q_{j1} + \lambda_i^4\left(\int_0^1 \phi_i^2 \mathrm{d}\overline{x}\right) q_{i0} \\
&- 2\sum_{j=1}^{n}\sum_{k=1}^{n}\left(\int_0^1 \phi_k\phi_j\phi_i \mathrm{d}\overline{x}\right)\lambda_j^4 q_{k0}q_{j0} + \sum_{j=1}^{n}\sum_{k=1}^{n}\sum_{l=1}^{n}\left(\int_0^1 \phi_l\phi_k\phi_j\phi_i \mathrm{d}\overline{x}\right)\lambda_j^4 q_{l0}q_{k0}q_{j0}
\end{aligned}$$

$$-\left(\overline{P}+\alpha\sum_{j=1}^{n}\sum_{k=1}^{n}\left(\int_0^1\phi_k{}'\phi_j{}'\mathrm{d}\overline{x}\right)q_{k0}q_{j0}\right)\left(\sum_{j=1}^{n}\left(\int_0^1\phi_j{}''\phi_i\mathrm{d}\overline{x}\right)q_{j0}-2\sum_{j=1}^{n}\sum_{k=1}^{n}\left(\int_0^1\phi_k\phi_j{}''\phi_i\mathrm{d}\overline{x}\right)q_{k0}q_{j0}\right.$$
$$\left.+\sum_{j=1}^{n}\sum_{k=1}^{n}\sum_{l=1}^{n}\left(\int_0^1\phi_l\phi_k\phi_j{}''\phi_i\mathrm{d}\overline{x}\right)q_{l0}q_{k0}q_{j0}\right)=\left(\overline{V_{\mathrm{DC}}}+\overline{V_{\mathrm{AC}}}\cos(\overline{\omega}\overline{t})\right)^2\left((1+\beta)\int_0^1\phi_i\mathrm{d}\overline{x}-\beta\left(\int_0^1\phi_i^2\mathrm{d}\overline{x}\right)q_{i0}\right)$$
$$\text{for } i=1,2,\ldots,n. \tag{43}$$

We solve numerically the $2n$ first-order differential equations Eqs. (42.1) and (43) by the commercial software MATLAB. The function ode45 based on an explicit Runge–Kutta method is used. The initial deflection and velocity are taken to be zero ($q_{i0}=q_{i1}=0$ at $\overline{t}=0$). Moreover, to obtain the steady-state solution, the equations are solved over a long period of time, i.e., $\overline{t}=0-2000$, so-called long-time integration. It is found in [34,35] that the reduced-order model using five modes can accurately describe the dynamic behavior of microbeams. So the first five vibration modes are taken here, i.e., $n=5$ in Eq. (39).

3 Results and discussions

3.1 Effects of applied voltages

Let us consider an electrically actuated microbeam of length $L=500\mu$m, thickness $h=10\mu$m, and an initial gap between it and the rigid electrode $g_0=2\ \mu$m. The applied voltages are: $V_{\mathrm{DC}}=2-70$ V, $V_{\mathrm{AC}}=0-2$ V. With the expressions in Table 1, and the material properties $E=160$ GPa, $\nu=0.27$ for silicon in [41], we calculate the values of the dimensionless quantities $\overline{V_{\mathrm{DC}}}$, $\overline{V_{\mathrm{AC}}}$, and α, as shown in Table 2. Using Table 2, we solve Eq. (35.1) at different levels of the detuning parameter δ and obtain the frequency responses of the microbeam at various levels of $\overline{V_{\mathrm{DC}}}$ and $\overline{V_{\mathrm{AC}}}$. The typical results are shown in Figs. 2 and 3.

Figure 2 is for a low $\overline{V_{\mathrm{DC}}}$ of 1. When $\overline{V_{\mathrm{AC}}}$ is small (e.g., 0.04 in Fig. 2a), the microbeam exhibits the linear frequency response: The maximum deflection changes gradually with the increase and decrease of the applied frequency. When $\overline{V_{\mathrm{AC}}}$ becomes larger (e.g., 0.1 in Fig. 2c), a typical hardening frequency response is observed. With the increase of the applied frequency $\overline{\omega}$, the maximum deflection increases gradually until reaching the first saddle-node bifurcation point SN1. A slight increase in $\overline{\omega}$ will lead to a sudden decrease of the maximum deflection, as depicted by SN1 $\rightarrow$ ① in Fig. 2c. During the decrease of $\overline{\omega}$, the maximum deflection increases gradually until reaching the second saddle-node bifurcation point SN2, where a slight decrease in $\overline{\omega}$ will cause a sudden increase in the maximum deflection, i.e., SN2 $\rightarrow$ ② in Fig. 2c. Similar observations have also been found from the experiments [17,23] and theoretical studies [20].

Figure 3 is for a relatively high $\overline{V_{\mathrm{DC}}}$ of 3.5. In this case, when $\overline{V_{\mathrm{AC}}}$ increases (e.g., 0.03 in Fig. 3c), a typical softening frequency response is observed. By increasing the applied frequency $\overline{\omega}$, the maximum deflection increases gradually until reaching SN1 where the maximum deflection suddenly increases, as indicated by SN1 $\rightarrow$ ① in Fig. 3c. When decreasing $\overline{\omega}$, the maximum deflection increases gradually until reaching SN2 where it suddenly decreases, see SN2 $\rightarrow$ ② in Fig. 3c. The experimental and theoretical investigations in [26] have similar observations.

Figures 2 and 3 show that $\overline{V_{\mathrm{AC}}}$ should be high enough for the microbeam to exhibit the nonlinear frequency responses. When $\overline{V_{\mathrm{AC}}}$ is low, the beam deflection is small, and as a result, the mid-plane stretching and the variation of the deflection-dependent electrostatic force are insignificant. In this case, the microbeam exhibits the linear frequency response. When $\overline{V_{\mathrm{AC}}}$ becomes high, the beam deflection increases, and the mid-plane

Table 2 Values of the dimensionless quantities

Quantity	Meaning	Value
$\overline{P}$	Dimensionless residual axial force	0 (no residual axial force)
Q	Quality factor	1000
$\overline{V_{\mathrm{AC}}}$	Dimensionless AC voltage amplitude	0–0.1
$\overline{V_{\mathrm{DC}}}$	Dimensionless DC voltage	0.1–3.5
α	Stretching parameter	0.24
β	Fringing field parameter	0 (no fringing field effect)

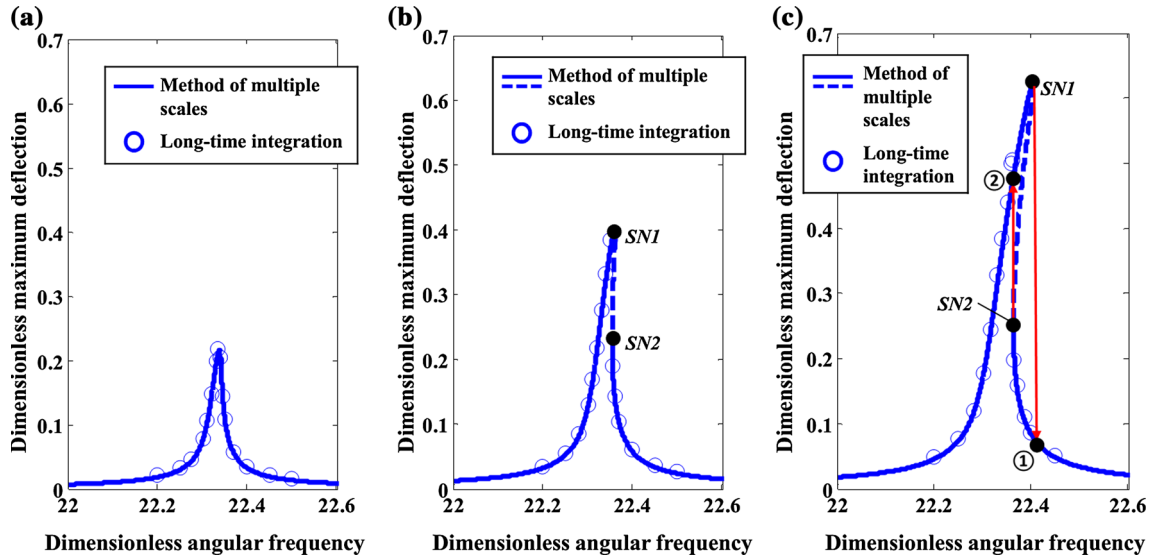

Fig. 2 Frequency response at different levels of AC voltage amplitude: **a** for linear frequency response, **b**, **c** for hardening frequency response. SN1 and SN2 are saddle-node bifurcation points. *Solid* and *dashed lines* are, respectively, the stable and unstable responses

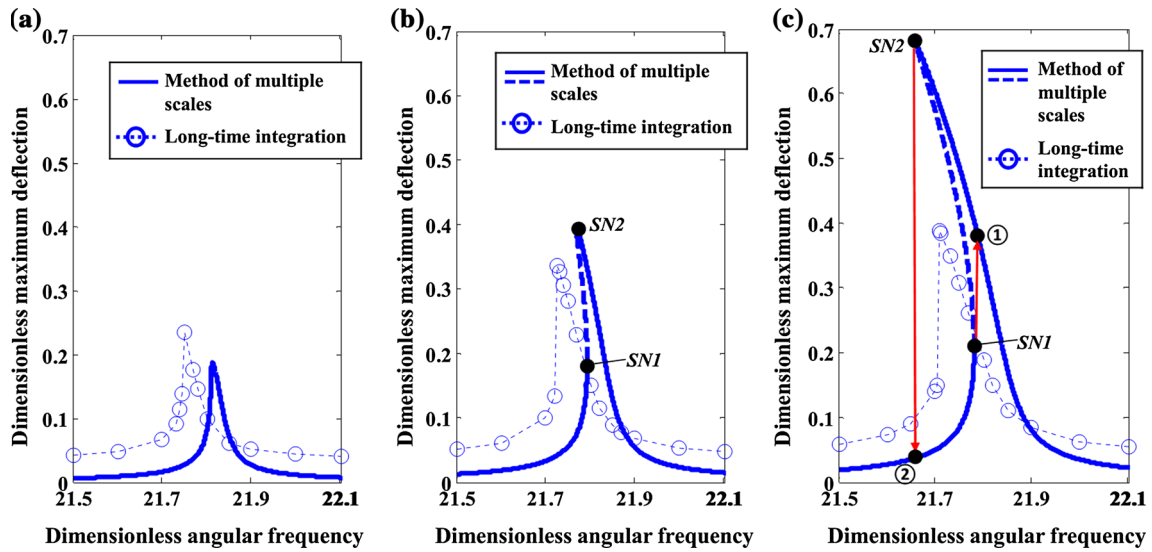

Fig. 3 Frequency response at different levels of AC voltage amplitude: **a** for linear frequency response, **b**, **c** for softening frequency response. Saddle nodes SN1 and SN2 are bifurcation points. *Solid* and *dashed lines* are, respectively, the stable and unstable responses

stretching (leading to a hardening effect on the microbeam) and the variation of electrostatic force (leading to a softening effect) become significant. Then the microbeam will exhibit the nonlinear frequency responses.

The numerical results from the long-time integration presented in Sect. 2.3 are also shown in Figs. 2 and 3, from which it is seen that the analytical model of Eq. (35.1) can capture the characteristic feature of the vibration behavior of the microbeam at the studied levels of DC and AC voltages. At low DC voltages (e.g., $\overline{V_{\mathrm{DC}}} = 1$ in Fig. 2), a quantitative agreement is found; while at high DC voltages (e.g., $\overline{V_{\mathrm{DC}}} = 3.5$ in Fig. 3), the increasing quantitative difference might be due to the fact that when $\overline{V_{\mathrm{DC}}}$ increases, the approximation of the electrostatic force in the analytical analysis becomes less accurate.

It is also found from Figs. 2 and 3 that whether the microbeam will exhibit the hardening or softening frequency response at high levels of AC voltage amplitude depends on the biased DC voltage. To study the effect of DC voltage on the existence of hardening and softening frequency responses, we solve Eq. (35.1)

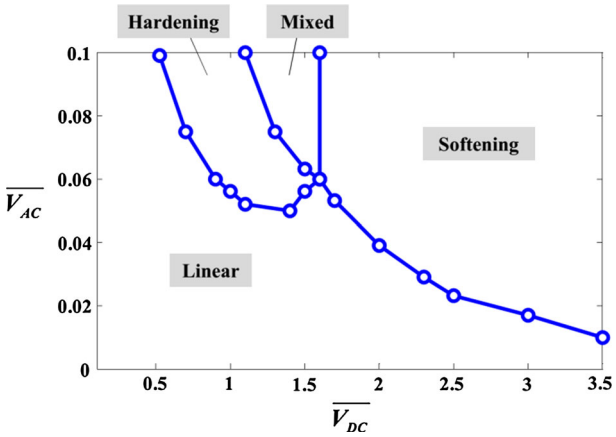

Fig. 4 Design domains identifying the characteristic feature of the vibration behavior of an electrically actuated clamped–clamped microbeam

with the parameters given in Table 2 and mark the characteristic feature of the obtained frequency response in a diagram in terms of $\overline{V_{\rm DC}}$ and $\overline{V_{\rm AC}}$, as shown in Fig. 4.

It is seen from Fig. 4 that when $\overline{V_{\rm DC}}$ is small (e.g., 1), the microbeam exhibits a hardening frequency response at high levels of $\overline{V_{\rm AC}}$, while at large $\overline{V_{\rm DC}}$ (e.g., 3), it exhibits a softening frequency response. As expected, larger $\overline{V_{\rm DC}}$ leads to a larger electrostatic force. Accordingly, the softening effect due to the electrostatic force becomes dominant at large values of $\overline{V_{\rm DC}}$, and the microbeam would exhibit a softening frequency response. At small values of $\overline{V_{\rm DC}}$, the hardening effect due to the mid-plane stretching becomes dominant, and a hardening frequency response can be observed. At $\overline{V_{\rm AC}} = 0.1$ (the highest level considered in this study), we determine the following critical values of $\overline{V_{\rm DC}}$ from Fig. 4: the maximum allowable $\overline{V_{\rm DC}} = 1.1$ for the existence of hardening frequency response and the minimum allowable $\overline{V_{\rm DC}} = 1.6$ for the existence of softening frequency response.

It is noted that the mixed domain in Fig. 4 is where the frequency response curve shows both the hardening and softening characteristics. It is also observed that when $\overline{V_{\rm DC}} = 1.1{-}2.5$, a discrepancy is found between the frequency responses obtained from the analytical model of Eq. (35.1) and those obtained from the numerical simulation in Sect. 2.3. The analytical model over-estimates the hardening effect and underestimates the softening effect, possibly due to the approximation of the electrostatic force. Therefore, in the region where $\overline{V_{\rm DC}} = 1.1{-}2.5$, the numerical simulation results are used to determine the vibration characteristics of the microbeam.

3.2 Effects of governing parameters

The dimensionless quantities in Table 2 are the parameters governing the vibration behavior of the microbeam. In Sect. 3.1, the effects of the electrical loading $\overline{V_{\rm DC}}$ and $\overline{V_{\rm AC}}$ are studied. In this Subsection, we examine the effects of other governing parameters, such as the stretching parameter α, the fringing field parameter β, the quality factor Q, and the dimensionless residual axial force $\overline{P}$. Moreover, the effects of boundary conditions are also investigated.

3.2.1 Stretching parameter

Except the stretching parameter α, we take the values of the other parameters in Table 2 and solve Eq. (35.1) at different levels of α. The obtained frequency response curves are depicted in Fig. 5. The hardening frequency response is observed at large values of α in Fig. 5a, while the softening frequency response is observed at small value of α in Fig. 5b. The stretching parameter α quantifies the effect of mid-plane stretching; i.e., by increasing α, the mid-plane stretching becomes more significant, which makes it easier for the microbeam to exhibit the hardening frequency response, while more difficult to exhibit the softening frequency response. As a result, the minimum $\overline{V_{\rm AC}}$ required to induce the hardening frequency response decreases when increasing α, and that is why the hardening frequency response is observed at large α in Fig. 5a. On the other hand, the

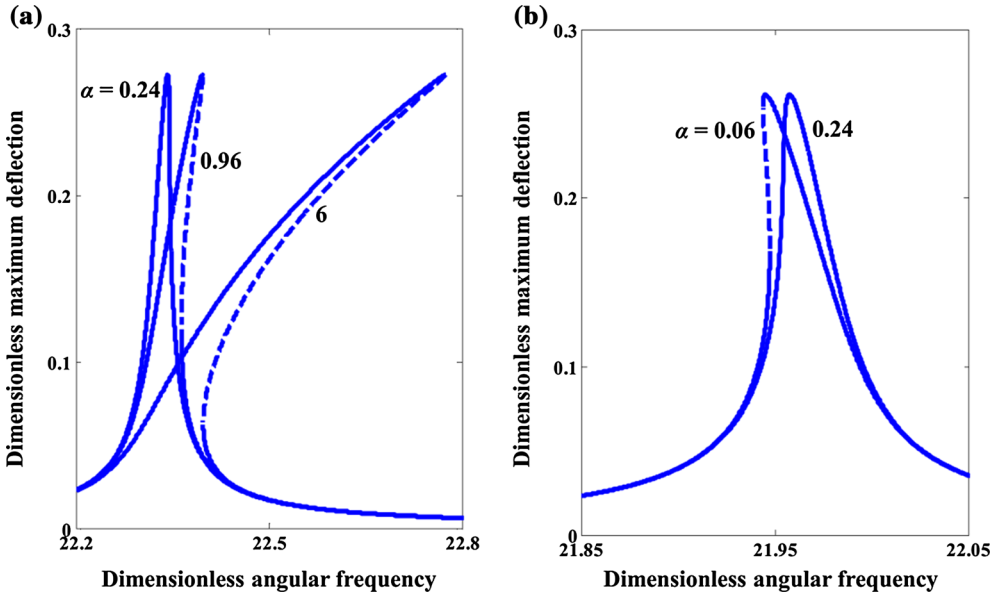

Fig. 5 Frequency response at different levels of stretching parameter α: **a** for $\overline{V_{\mathrm{DC}}} = 1$, $\overline{V_{\mathrm{AC}}} = 0.05$; **b** for $\overline{V_{\mathrm{DC}}} = 3$, $\overline{V_{\mathrm{AC}}} = 0.016$. *Solid* and *dashed lines* are, respectively, the stable and unstable responses

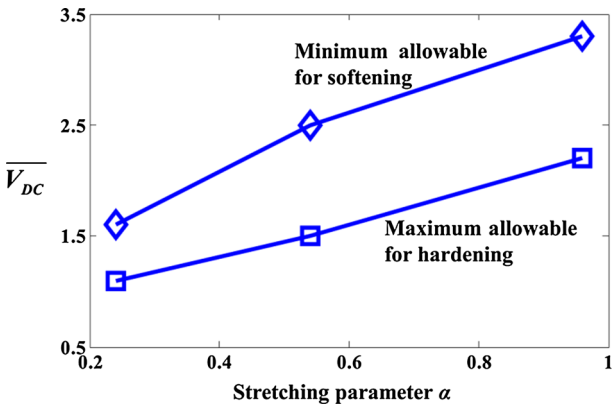

Fig. 6 Maximum allowable $\overline{V_{\mathrm{DC}}}$ for the existence of hardening frequency response and minimum allowable $\overline{V_{\mathrm{DC}}}$ for the existence of softening frequency response: effect of stretching parameter α

minimum $\overline{V_{\mathrm{AC}}}$ required for the softening frequency response increases with the increase of α, so the softening frequency response is only observed at small α in Fig. 5b. The expression in Table 1 indicates that we can adjust the value of α by varying the beam thickness h and/or the initial gap g_0 between the beam and the electrode.

Using the numerical simulation presented in Sect. 2.3, we obtain the critical values of $\overline{V_{\mathrm{DC}}}$ at different levels of α in Fig. 6. The critical values are: the maximum allowable $\overline{V_{\mathrm{DC}}}$ for the existence of hardening frequency response and the minimum allowable $\overline{V_{\mathrm{DC}}}$ for the existence of softening frequency response. It is found from Fig. 6 that with the increase of α both critical values of $\overline{V_{\mathrm{DC}}}$ increase. This indicates that the hardening domain expands at the expense of the softening domain in the design diagram of Fig. 4. This is because increasing α strengthens the hardening effect.

3.2.2 Fringing field parameter

The fringing field effect due to the finite size of the beam width b is described by a fringing field parameter β, which is equal to $0.65 g_0/b$ from Table 1. In order to make use of Palmer's formula to estimate the fringing field in this study, the microbeam system must satisfy the inequality $b > 10 g_0$ [32]. For the narrow beams

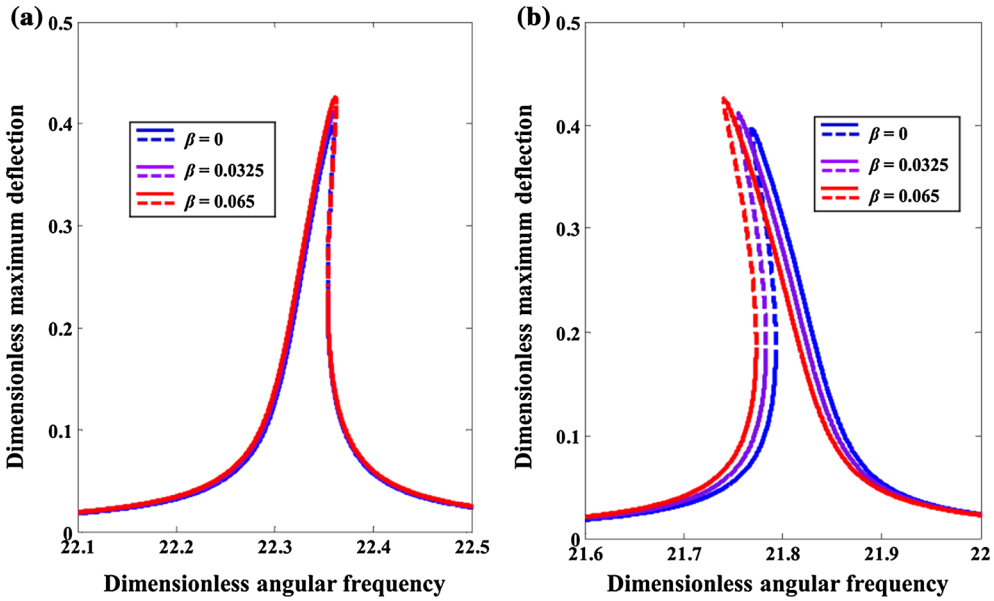

Fig. 7 Frequency response at different levels of fringing field parameter β: **a** for hardening frequency response and **b** for softening frequency response. *Solid* and *dashed lines* are, respectively, the stable and unstable responses

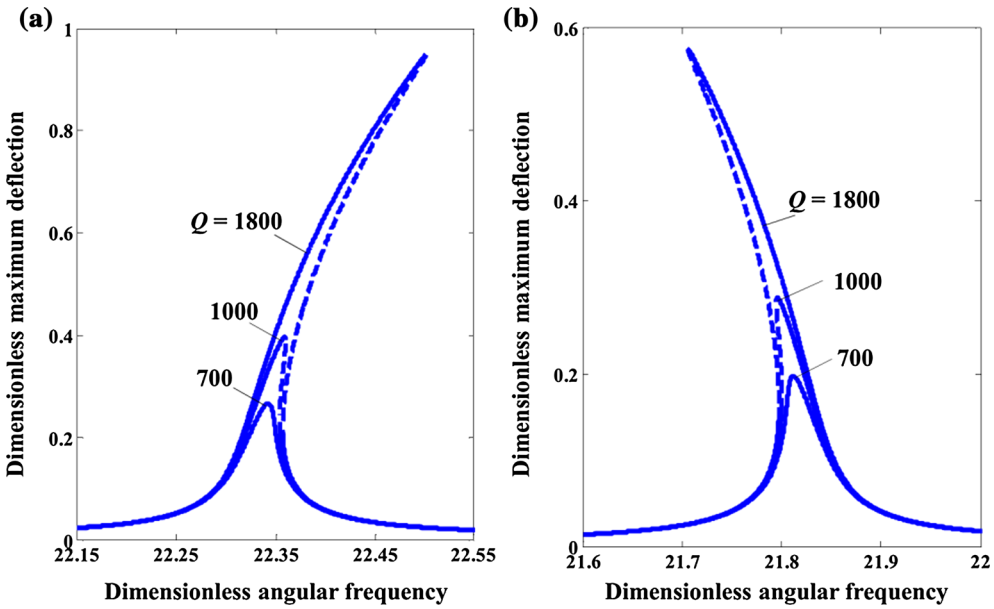

Fig. 8 Frequency response at different levels of quality factor Q: **a** for $\overline{V_{\mathrm{DC}}} = 1$, $\overline{V_{\mathrm{AC}}} = 0.07$; **b** for $\overline{V_{\mathrm{DC}}} = 3.5$, $\overline{V_{\mathrm{AC}}} = 0.015$. *Solid* and *dashed lines* are, respectively, the stable and unstable responses

of smaller width, more complicated formulae such as [42,43] should be used. Here we have: $\beta = 0{-}0.065$. Using Eq. (35.1) and Table 2, the frequency responses at different levels of β are depicted in Fig. 7. It is seen from the Figure that the effect of β at the studied level is insignificant.

3.2.3 Quality factor

Figure 8 shows the frequency response of the microbeam at different levels of the quality factor Q, which are obtained using Eq. (35.1) and Table 2. The figure indicates that increasing Q strengthens both the hardening and softening effects, so the minimum $\overline{V_{\mathrm{AC}}}$ required to induce the nonlinear frequency responses decreases with the increase of Q, and as a result, the nonlinear frequency responses are observed at large values of

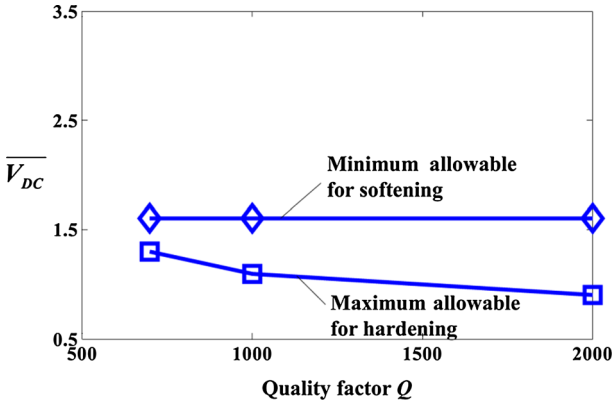

Fig. 9 Maximum allowable $\overline{V_{\mathrm{DC}}}$ for the existence of hardening frequency response and minimum allowable $\overline{V_{\mathrm{DC}}}$ for the existence of softening frequency response: effect of quality factor Q

Q in Fig. 8. The quality factor Q is inversely proportional to the dimensionless damping coefficient $\overline{c_{\mathrm{d}}}$, as shown in Eq. (37). Therefore, increasing Q reduces the damping effect, which leads to an increase in the beam deflection. In this case, the nonlinear effects due to mid-plane stretching and electrostatic force become more significant, and consequently, smaller $\overline{V_{\mathrm{AC}}}$ is needed to induce the nonlinear frequency responses.

Using the numerical simulation results, we determine the maximum allowable $\overline{V_{\mathrm{DC}}}$ for the existence of hardening frequency response and the minimum allowable $\overline{V_{\mathrm{DC}}}$ for the existence of softening frequency response and show these two critical values of $\overline{V_{\mathrm{DC}}}$ at different levels of the quality factor Q in Fig. 9. It is seen that Q has a minor effect on these critical values of $\overline{V_{\mathrm{DC}}}$. If the hardening effect is strengthened compared to the softening effect, the critical values of $\overline{V_{\mathrm{DC}}}$ will increase, indicating that the hardening domain expands at the expense of the softening domain in the design diagram of Fig. 4. Similarly, the critical values of $\overline{V_{\mathrm{DC}}}$ will decrease if the softening effect is strengthened compared to the hardening effect. Since both hardening and softening effects are equally strengthened by increasing Q, the critical values of $\overline{V_{\mathrm{DC}}}$ remain unchanged.

3.2.4 Residual axial force

The frequency response at different levels of dimensionless residual axial force $\overline{P}$, using Eq. (35.1) and Table 2, is obtained and shown in Fig. 10. It is seen from the Figure that the axial compressive force ($\overline{P} < 0$ in Fig. 10) strengthens the hardening and softening effects on the microbeam, while the axial tensile force ($\overline{P} > 0$) weakens them. The compressive force increases the beam deflection, and as a result, the nonlinear effects from mid-plane stretching and electrostatic force become significant. The tensile force has the opposite influence. So the compressive force reduces the minimum $\overline{V_{\mathrm{AC}}}$ required to induce the nonlinear frequency responses, while the tensile force increases them. And that is why the nonlinear frequency responses are observed at the compressive force in Fig. 10.

From the numerical simulation results, the maximum allowable $\overline{V_{\mathrm{DC}}}$ for the existence of hardening frequency response and the minimum allowable $\overline{V_{\mathrm{DC}}}$ for the existence of softening frequency response are obtained. It is seen from Fig. 11 that these two critical values of $\overline{V_{\mathrm{DC}}}$ are only slightly affected by the dimensionless residual axial force $\overline{P}$. The hardening and softening effects are equally strengthened or weakened by $\overline{P}$. Therefore, $\overline{P}$ has an insignificant effect on the critical values of $\overline{V_{\mathrm{DC}}}$.

3.2.5 Boundary conditions

The previous studies are conducted on a clamped–clamped microbeam. However, the beam can be subjected to other boundary conditions such as simply supported and cantilever. In this Subsection, we investigate the effects of the boundary conditions on the frequency response of the microbeam.

Let us consider a simply supported microbeam depicted in Fig. 12a first. Its axial displacements at the boundaries are the same as those of the clamped–clamped beam, i.e., $u(0) = u(L) = 0$. Accordingly, the axial force can be calculated by (13), and the governing equation (15) can be used. We further take the first linear undamped vibration mode ϕ_1 of the simply supported beam:

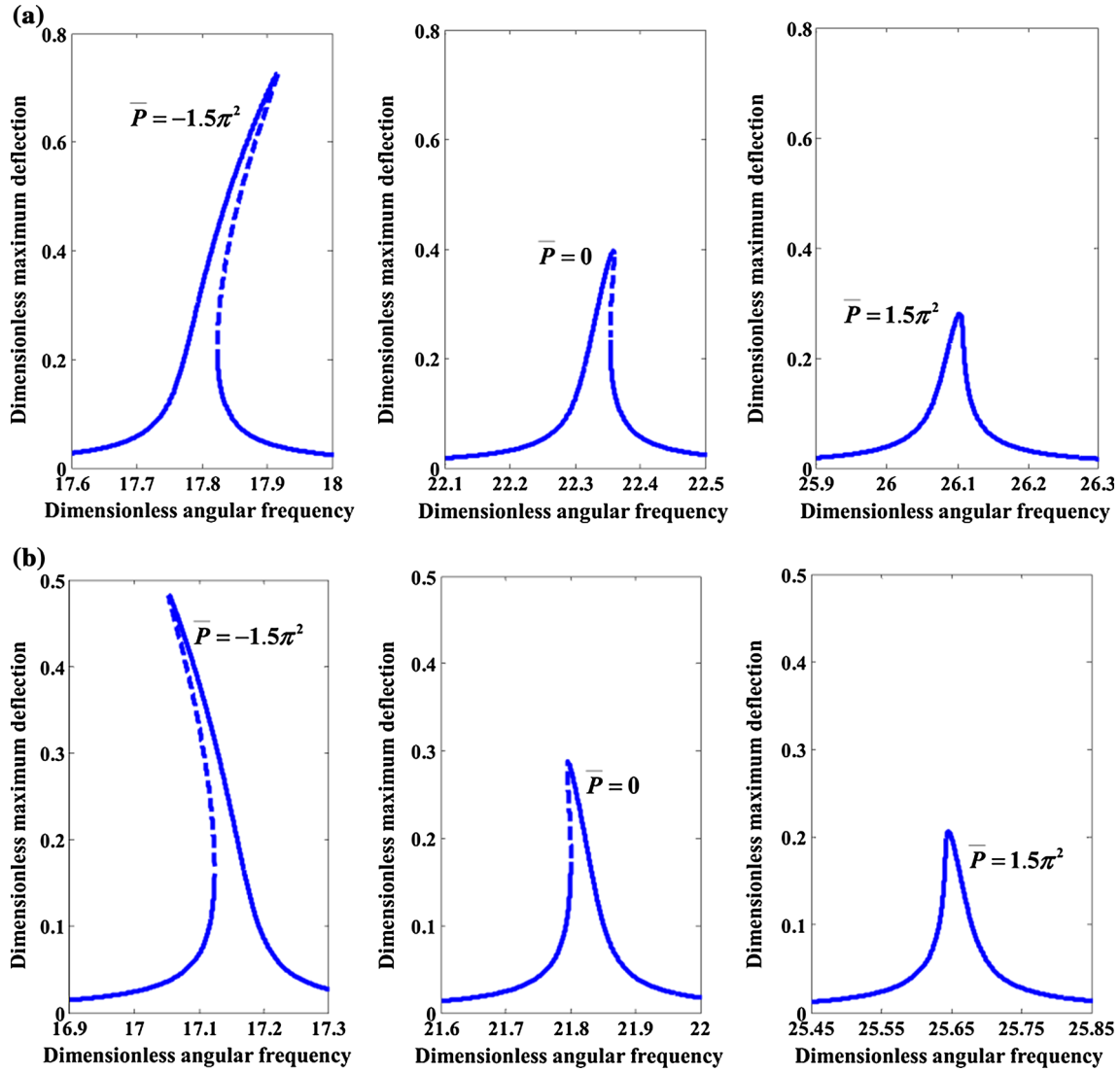

Fig. 10 Frequency response at different levels of dimensionless residual axial force $\overline{P}$: **a** for hardening frequency response ($\overline{V_{DC}} = 1$, $\overline{V_{AC}} = 0.07$) and **b** for softening frequency response ($\overline{V_{DC}} = 3.5$, $\overline{V_{AC}} = 0.015$). *Solid* and *dashed lines* are, respectively, the stable and unstable responses

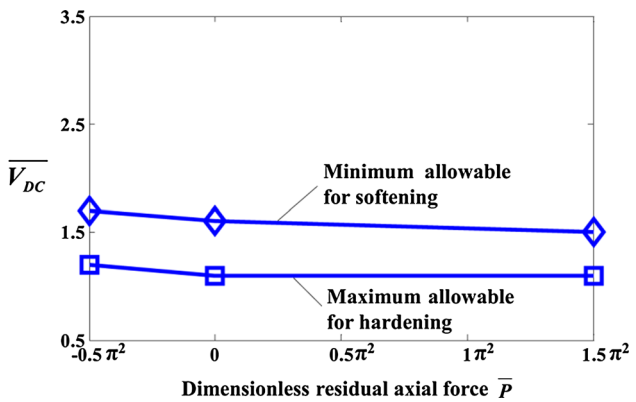

Fig. 11 Maximum allowable $\overline{V_{DC}}$ for the existence of hardening frequency response and minimum allowable $\overline{V_{DC}}$ for the existence of softening frequency response: effect of dimensionless residual axial force $\overline{P}$

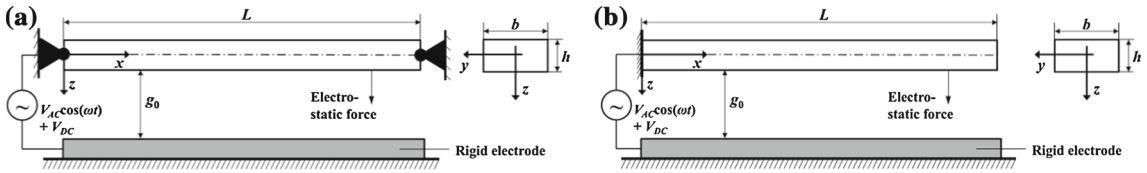

Fig. 12 Microbeam subjected to different boundary conditions: **a** simply supported, **b** cantilever

$$\phi_1(\overline{x}) = \sin(\pi \overline{x}) \tag{44}$$

with the frequency parameter $\lambda_1 = \pi$ and follow the similar procedures in Sect. 2.2 to obtain Eq. (35.1) for studying the frequency response of the simply supported microbeam.

Let us now consider a cantilever-type microbeam that is anchored at one end, as depicted in Fig. 12b. The axial force at the free end of the cantilever microbeam is zero. Then from Eq. (10.1) we obtain:

$$N(x, t) = 0. \tag{45}$$

Introducing Eqs. (6), (7), (12.2), and (45) into Eq. (10.2), we have:

$$\rho S \frac{\partial^2 w}{\partial t^2} + c_{\mathrm{d}} \frac{\partial w}{\partial t} + E^* I \frac{\partial^4 w}{\partial x^4} = \frac{1}{2} \frac{\varepsilon_0 b \left(V_{\mathrm{DC}} + V_{\mathrm{AC}} \cos(\omega t)\right)^2}{(g_0 - w)^2} \left(1 + 0.65 \frac{g_0 - w}{b}\right). \tag{46}$$

Then the following dimensionless governing equation can be obtained using Table 1 and Eq. (46):

$$\frac{\partial^2 \overline{w}}{\partial \overline{t}^2} + \overline{c_{\mathrm{d}}} \frac{\partial \overline{w}}{\partial \overline{t}} + \frac{\partial^4 \overline{w}}{\partial \overline{x}^4} = \left(\overline{V_{\mathrm{DC}}} + \overline{V_{\mathrm{AC}}} \cos(\overline{\omega} \overline{t})\right)^2 \left(\frac{1}{(1 - \overline{w})^2} + \frac{\beta}{(1 - \overline{w})}\right). \tag{47}$$

It is seen that Eq. (47) does not include the mid-plane stretching term with the stretching parameter α. So the cantilever microbeam cannot exhibit the hardening frequency response. Using the first linear undamped vibration mode ϕ_1 of the cantilever beam:

$$\phi_1(\overline{x}) = C_1 \left(\cos h(\lambda_1 \overline{x}) - \cos(\lambda_1 \overline{x}) - \frac{\sin h(\lambda_1) - \sin(\lambda_1)}{\cos h(\lambda_1) + \cos(\lambda_1)} \left(\sin h(\lambda_1 \overline{x}) - \sin(\lambda_1 \overline{x})\right)\right) \tag{48}$$

with C_1 satisfying $\max_{\overline{x} \in [0,1]} |\phi_1(\overline{x})| = 1$ and λ_1 satisfying $\cos h(\lambda_1) \cos(\lambda_1) = -1$, and following the procedures in Sect. 2.2, we arrive at a similar expression to Eq. (35.1). The only difference is that the coefficient b_3 in Eq. (35.1) is modified to be $\frac{3m_4}{8m_2\omega_1} (4 + \beta) \overline{V_{\mathrm{DC}}}^2$.

Using Table 2 and Eq. (35.1), we obtain the frequency responses of the microbeam under different boundary conditions. The results of the cantilever-type microbeam are shown in Fig. 13. As expected, the cantilever microbeam can only exhibit the nonlinear frequency response of softening characteristic. Figure 14 compares the frequency responses of simply supported and clamped–clamped microbeams. It is seen from the Figure that the hardening and softening effects in the simply supported microbeam are more significant than those in the clamped–clamped beam. The reduced rotation at the two ends of the clamped–clamped microbeam makes it more difficult to bend, and as a result, the clamped–clamped beam has a smaller deflection, which leads to the weaker nonlinear effects from mid-plane stretching and electrostatic force. Therefore, higher $\overline{V_{\mathrm{AC}}}$ is required to induce the nonlinear frequency responses of the clamped–clamped microbeam. That is why the nonlinear frequency responses are only observed in the simply supported microbeam in Fig. 14.

It is noted that at $\overline{V_{\mathrm{AC}}} = 0.1$ and $\overline{V_{\mathrm{DC}}} > 0.7$ a transient dimensionless deflection reaching 1 is predicted by the numerical simulation near the primary resonance regime of the simply supported microbeam. This indicates that the simply supported microbeam will collapse onto the rigid electrode and cannot exhibit the vibration behavior. In this case, we cannot determine the maximum allowable $\overline{V_{\mathrm{DC}}}$ for the existence of hardening frequency response and the minimum allowable $\overline{V_{\mathrm{DC}}}$ for the existence of softening frequency response of the simply supported microbeam at $\overline{V_{\mathrm{AC}}} = 0.1$.

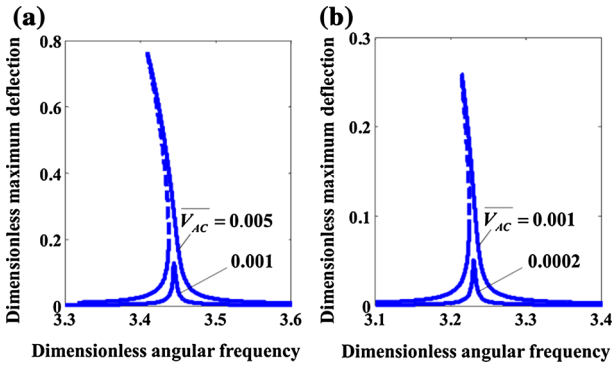

Fig. 13 Frequency response of a cantilever-type microbeam: **a** for $\overline{V_{\mathrm{DC}}} = 0.5$ and **b** for $\overline{V_{\mathrm{DC}}} = 1$. *Solid* and *dashed lines* are the respective stable and unstable responses

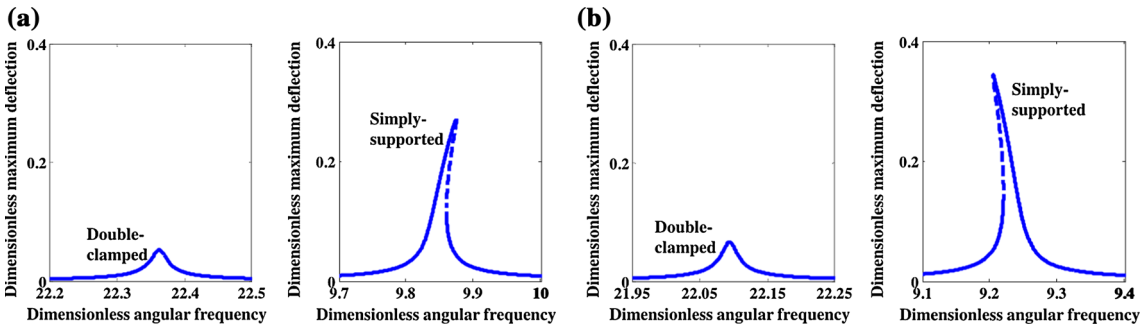

Fig. 14 Frequency responses of double-clamped and simply supported microbeams: **a** for low $\overline{V_{\mathrm{DC}}}$ ($\overline{V_{\mathrm{DC}}} = 0.5$, $\overline{V_{\mathrm{AC}}} = 0.02$)) and **b** for high $\overline{V_{\mathrm{DC}}}$ ($\overline{V_{\mathrm{DC}}} = 2.5$, $\overline{V_{\mathrm{AC}}} = 0.005$)). *Solid* and *dashed lines* are the respective stable and unstable responses

4 Conclusions

This paper investigates the vibration behavior of an electrically actuated microbeam under various levels of DC and AC voltages. The governing equations are developed in the framework of Euler–Bernoulli beam theory, accounting for the effects of mid-plane stretching, fringing field, damping and residual axial force. The equations are solved by the method of multiple scales and used to derive the frequency response of the microbeam under different boundary conditions.

Our results reveal that the characteristic feature of the frequency response of the microbeam highly depends on the applied AC and DC voltages. Large AC voltage amplitude is required to induce the nonlinear frequency response, and the biased DC voltage determines whether the microbeam will exhibit hardening or softening frequency response. A design chart in terms of the dimensionless DC voltage and AC voltage amplitude is further developed to show the domains of characteristic frequency responses. Moreover, our results reveal the significant effects of the mid-plane stretching, damping, residual axial force, and boundary conditions on the minimum required AC voltage amplitudes for the nonlinear frequency responses, while only the mid-plane stretching influences the critical DC voltages separating the hardening and softening frequency response regions in the design chart of the micro-resonator.

Acknowledgements The financial support provided by the Natural Sciences and Engineering Research Council of Canada and the Discovery Accelerator Supplements is gratefully acknowledged.

References

1. Brown, E.R.: RF-MEMS switches for reconfigurable integrated circuits. IEEE Trans. Microw. Theory **46**, 1868–1880 (1998)
2. Rueckes, T., Kim, K., Joselevich, E., Tseng, G.Y., Cheung, C.-L., Lieber, C.M.: Carbon nanotube-based nonvolatile random access memory for molecular computing. Science **289**, 94–97 (2000)
3. Charlot, B., Sun, W., Yamashita, K., Fujita, H., Toshiyoshi, H.: Bistable nanowire for micromechanical memory. J. Micromech. Microeng. **18**, 045005 (2008)

4. Jang, J.E., Cha, S.N., Choi, Y.J., Kang, D.J., Butler, T.P., Hasko, D.G., Jung, J.E., Kim, J.M., Amaratunga, G.A.J.: Nanoscale memory cell based on a nanoelectromechanical switched capacitor. Nat. Nanotechnol. **3**, 26–30 (2008)
5. Roodenburg, D., Spronck, J.W., Van der Zant, H.S.J., Venstra, W.J.: Buckling beam micromechanical memory with on-chip readout. Appl. Phys. Lett. **94**, 183501 (2009)
6. Intaraprasonk, V., Fan, S.: Nonvolatile bistable all-optical switch from mechanical buckling. Appl. Phys. Lett. **98**, 241104 (2011)
7. Mohanty, P.: Nano-oscillators get it together. Nature **437**, 325–326 (2005)
8. Peng, H.B., Chang, C.W., Aloni, S., Yuzvinsky, T.D., Zettl, A.: Ultrahigh frequency nanotube resonators. Phys. Rev. Lett. **97**, 087203 (2006)
9. Yang, Y.T., Callegari, C., Feng, X.L., Ekinci, K.L., Roukes, M.L.: Zeptogram-scale nanomechanical mass sensing. Nano Lett. **6**, 583–586 (2006)
10. Burg, T.P., Godin, M., Knudsen, S.M., Shen, W., Carlson, G., Foster, J.S., Babcock, K., Manalis, S.R.: Weighing of biomolecules, single cells and single nanoparticles in fluid. Nature **446**, 1066–1069 (2007)
11. Hopcroft, M.A., Kim, B., Chandorkar, S., Melamud, R., Agarwal, M., Jha, C.M., Bahl, G., Salvia, J., Mehta, H., Lee, H.K., Candler, R.N., Kenny, T.W.: Using the temperature dependence of resonator quality factor as a thermometer. Appl. Phys. Lett. **91**, 013505 (2007)
12. Chiu, H.-Y., Hung, P., Postma, H.W.C., Bockrath, M.: Atomic-scale mass sensing using carbon nanotube resonators. Nano Lett. **8**, 4342–4346 (2008)
13. Kwon, T., Eom, K., Park, J., Yoon, D.S., Lee, H.L., Kim, T.S.: Micromechanical observation of the kinetics of biomolecular interactions. Appl. Phys. Lett. **93**, 173901 (2008)
14. Southworth, D.R., Bellan, L.M., Linzon, Y., Craighead, H.G., Parpia, J.M.: Stress-based vapor sensing using resonant microbridges. Appl. Phys. Lett. **96**, 163503 (2010)
15. Chaste, J., Eichler, A., Moser, J., Ceballos, G., Rurali, R., Bachtold, A.: A nanomechanical mass sensor with yoctogram resolution. Nat. Nanotechnol. **7**, 301–304 (2012)
16. Wang, Q., Arash, B.: A review on applications of carbon nanotubes and graphenes as nano-resonator sensors. Comput. Mater. Sci. **82**, 350–360 (2014)
17. Tilmans, H.A.C., Legtenberg, R.: Electrostatically driven vacuum-encapsulated polysilicon resonators Part II. Theory and performance. Sens. Actuators A **45**, 67–84 (1994)
18. Kuang, J.-H., Chen, C.-J.: Dynamic characteristics of shaped micro-actuators solved using the differential quadrature method. J. Micromech. Microeng. **14**, 647–655 (2004)
19. Jonsson, L.M., Axelsson, S., Nord, T., Viefers, S., Kinaret, J.M.: High frequency properties of a CNT-based nanorelay. Nanotechnology **15**, 1497–1502 (2004)
20. Jia, X.L., Yang, J., Kitipornchai, S., Lim, C.W.: Resonance frequency response of geometrically nonlinear micro-switches under electrical actuation. J. Sound Vib. **331**, 3397–3411 (2012)
21. Zook, J.D., Burns, D.W., Guckel, H., Sniegowski, J.J., Engelstad, R.L., Feng, Z.: Characteristics of polysilicon resonant microbeams. Sens. Actuators A **35**, 51–59 (1992)
22. Carr, D.W., Evoy, S., Sekaric, L., Craighead, H.G., Parpia, J.M.: Measurement of mechanical resonance and losses in nanometer scale silicon wires. Appl. Phys. Lett. **75**, 920–922 (1999)
23. Evoy, S., Carr, D.W., Sekaric, L., Olkhovets, A., Parpia, J.M., Craighead, H.G.: Nanofabrication and electrostatic operation of single-crystal silicon paddle oscillators. J. Appl. Phys. **86**, 6072–6077 (1999)
24. Badzey, R.L., Zolfagharkhani, G., Gaidarzhy, A., Mohanty, P.: A controllable nanomechanical memory element. Appl. Phys. Lett. **85**, 3587–3589 (2004)
25. Almog, R., Zaitsev, S., Shtempluck, O., Buks, E.: Noise squeezing in a nanomechanical duffing resonator. Phys. Rev. Lett. **98**, 078103 (2007)
26. Mestrom, R.M.C., Fey, R.H.B., Van Beek, J.T.M., Phan, K.L., Nijmeijer, H.: Modelling the dynamics of a MEMS resonator: simulations and experiments. Sens. Actuators A **142**, 306–315 (2008)
27. Alsaleem, F.M., Younis, M.I., Ouakad, H.M.: On the nonlinear resonances and dynamic pull-in of electrostatically actuated resonators. J. Micromech. Microeng. **19**, 045013 (2009)
28. Ruzziconi, L., Bataineh, A.M., Younis, M.I., Cui, W., Lenci, S.: Nonlinear dynamics of an electrically actuated imperfect microbeam resonator: experimental investigation and reduced-order modeling. J. Micromech. Microeng. **23**, 075012 (2013)
29. Gui, C., Legtenberg, R., Tilmans, H.A.C., Fluitman, J.H.J., Elwenspoek, M.: Nonlinearity and hysteresis of resonant strain gauges. J. Microelectromech. Syst. **7**, 122–127 (1998)
30. Rhoads, J.F., Shaw, S.W., Turner, K.L.: The nonlinear response of resonant microbeam systems with purely-parametric electrostatic actuation. J. Micromech. Microeng. **16**, 890–899 (2006)
31. Kacem, N., Baguet, S., Hentz, S., Dufour, R.: Computational and quasi-analytical models for non-linear vibrations of resonant MEMS and NEMS sensors. Int. J. Nonlinear Mech. **46**, 532–542 (2011)
32. Caruntu, D.I., Knecht, M.W.: On nonlinear response near-half natural frequency of electrostatically actuated microresonators. Int. J. Struct. Stab. Dyn. **11**, 641–672 (2011)
33. Caruntu, D.I., Martinez, I., Knecht, M.W.: Reduced order model analysis of frequency response of alternating current near half natural frequency electrostatically actuated MEMS cantilevers. J. Comput. Nonlinear Dyn. **8**, 031011 (2013)
34. Caruntu, D.I., Martinez, I.: Reduced order model of parametric resonance of electrostatically actuated MEMS cantilever resonators. Int. J. Nonlinear Mech. **66**, 28–32 (2014)
35. Ouakad, H.M., Younis, M.I.: The dynamic behavior of MEMS arch resonators actuated electrically. Int. J. Nonlinear Mech. **45**, 704–713 (2010)
36. Kim, I.K., Lee, S.I.: Theoretical investigation of nonlinear resonances in a carbon nanotube cantilever with a tip-mass under electrostatic excitation. J. Appl. Phys. **114**, 104303 (2013)
37. Reddy, J.N.: Microstructure-dependent couple stress theories of functionally graded beams. J. Mech. Phys. Solids **59**, 2382–2399 (2011)

38. Palmer, H.B.: The capacitance of a parallel-plate capacitor by the Schwartz–Christoffel transformation. Trans. Am. Inst. Electr. Eng. **56**, 363–366 (1937)
39. Gupta, R.K.: Electrostatic Pull-In Test Structure Design for In-Situ Mechanical Property Measurements of Microelectromechanical Systems (MEMS). Massachusetts Institute of Technology, Cambridge (1997)
40. Nayfeh, A.H., Younis, M.I., Abdel-Rahman, E.M.: Dynamic pull-in phenomenon in MEMS resonators. Nonlinear Dyn. **48**, 153–163 (2007)
41. Zhang, Y., Wang, Y., Li, Z., Huang, Y., Li, D.: Snap-through and pull-in instabilities of an arch-shaped beam under an electrostatic loading. J. Microelectromech. Syst. **16**, 684–693 (2007)
42. Van der Meijs, N.P., Fokkema, J.T.: VLSI circuit reconstruction from mask topology. Integr. VLSI J. **2**, 85–119 (1984)
43. Batra, R.C., Porfiri, M., Spinello, D.: Electromechanical model of electrically actuated narrow microbeams. J. Microelectromech. Syst. **15**, 1175–1189 (2006)